Supplementary Information

Observation of Pull in Instability of Graphene Membranes under Interfacial Force

*Xinghui Liu[1], Narasimha G. Boddeti[1], Mariah R. Szpunar[2], Luda Wang[1], Miguel A. Rodriguez[3], Rong Long[1,4], Jianliang Xiao[1], Martin L. Dunn[5], and J. Scott Bunch[1]**

[1]Department of Mechanical Engineering, University of Colorado, Boulder, CO 80309 USA

[1]Department of Mechanical Engineering, University of Colorado, Boulder, CO 80309 USA

[2]Department of Mechanical Engineering, University of Miami, Coral Gables, FL 33124 USA

[3]Department of Mechanical Engineering, Columbia University, New York, NY 10027

[4]Department of Mechanical Engineering, University of Alberta, Edmonton, Alberta T6G 2G8, Canada

[5]Singapore University of Technology and Design, Singapore, 138682

*email: jbunch@colorado.edu

Fabrication Processes

Suspended graphene membranes were fabricated by a combination of standard photolithography, reactive ion etching and mechanical exfoliation of graphene. An array of annular cavities with designed dimensions was first defined by photolithography on an oxidized silicon wafer with a silicon oxide thickness of 90/285 nm. Reactive ion etching was then used to etch the annular rings into microcavities with a depth of 100-120 nm. After removal of photoresist with acetone and isopropanol, the chips were further cleaned in a Nanostrip bath at 60°C for 20 minutes. Thermal evaporation is used to deposit a layer of Cr/Au 5/10 nm for the Au coated annular rings. During the evaporation process, the chips are tilted at a 10~15° angle, so that the Cr/Au atoms can be deposited into the annular rings and cover the side walls. The large aspect ratio between the width and depth of the annular ring allows for a conformal metal deposition such that the post and the substrate are electrically contacted and grounded. Mechanical exfoliation of natural graphite using Scotch tape was then used to deposit suspended graphene sheets over the microcavities.

The pull-in distances in Fig. 1e were measured from two graphene flakes about 100 μm apart from each other on the same chip (Fig. S1). In the two graphene flakes, there were 13 one-layer, 9 two-layer, 5 three-layer, 5 four-layer, and 3 five-layer suspended membranes. For both the graphene/SiO_x and the graphene/Au annular rings, the number of graphene layers was verified using Raman spectroscopy and optical contrast.

Counting the Number of Graphene Layers

In order to count the number of graphene layers used in this study, we used optical contrast verified by Raman spectroscopy. Figure S1 (a) shows a graphene flake used in this study. The devices in Figure S1 (a) correspond to the devices in Figure 1e. The corresponding spots where Raman spectrum was taken for each device are shown as colored circles; red is 1 layer, green is 2 layers, blue is 3 layers, cyan is 4 layers and magenta is 5 layers. Figures S1 (b) shows the Raman spectrum taken from the spots of corresponding color in S1 (a), respectively. To verify the number of layers we found the ratio of the integrated intensity of the first order optical phonon peak and the graphene G peak (Fig. S1 (c))[1].

To measure the Raman spectrum on the gold coated samples, we patterned areas that contained no Au/Cr over which Raman spectrum of the graphene was taken without interference from the gold film. We patterned 5 μm circular discs between the annular wells using photolithography which masked the subsequent thermal evaporation of Au/Cr onto the SiO_x. After evaporation and lift-off, the protected areas contained no Au/Cr while all other areas of the wafer were covered with the Au/Cr film. We then used mechanical exfoliation to deposit the graphene and took the Raman spectrum of graphene through the 5 μm circular wells similarly to Fig S1. Figure S2 (a) shows a few layer graphene flake on Au/Cr coated wafer. The larger circles are locations where there is no Au/Cr and only SiO_x with or without graphene. The blue circle corresponds to the

location where Raman spectrum was taken. The number of graphene layers is verified using the same method as previously introduced.

Analytical Model

We developed a simple analytical model based on membrane mechanics to describe the interrelationship of the system parameters in the experiment and we use it inversely with the measurements to infer the operant surface forces[2].

The symbols used in our approach are:

b = Post radius

a = Outer radius of the cavity

E = Young's Modulus

t = Thickness

v = Poisson's Ratio

S = Total tension/membrane force in the radial direction

S_r = Incremental tension in the radial direction

S_t = Incremental tension in the tangential direction

S_0 = Initial equi-biaxial tension

ΔP = Pressure exerted by the difference of gas pressures inside and outside the cavity

P_{att} = Pressure due to the post-graphene interactions

r = Radial co-ordinate, $0 < r <$ a

w = Deflection of the membrane, as a function of r

h = Deflection at $r = 0$

The key assumptions of our treatment are:

1) The membrane tension S is uniform.
2) The pressure due to the surface forces acting between the post and the membrane, $P_{att,}$ is uniform. This is reasonable if the membrane curvature is small. This is the case when the post is small compared to the overall size of the cavity.

In order to understand the validity and impact of these assumptions, we also carry out high-fidelity finite element (FE) simulations where they are removed; these are described in the next section.

Force equilibrium in the vertical direction gives (see Figure S3 (a)):

$$(\Delta P - P_{att})r^2 = -2\,S\,r\frac{dw}{dr} \qquad r < b$$

$$\Delta P\,r^2 - P_{att}b^2 = -2\,S\,r\frac{dw}{dr} \qquad r \geq b$$

$$S = S_r + S_0$$

The negative sign on the right hand side is due to dw/dr being negative. Integrating with respect to r with appropriate limits, yields:

$$w = h - \frac{\Delta P - P_{att}}{4S}r^2 \qquad r < b$$

$$w = w(r = b) + \frac{1}{4S}\left(P_{att}b^2 log\left(\frac{r^2}{b^2}\right) - \Delta P(r^2 - b^2)\right) \qquad r \geq b$$

Due to continuity of w at $r = b$ we obtain:

$$w = h - \frac{\Delta P - P_{att}}{4S} r^2 \qquad r < b$$

$$w = h + \frac{1}{4S}\left(P_{att} b^2 log\left(\frac{r^2}{b^2}\right) + P_{att} b^2 - \Delta P\, r^2 \right) \qquad r \geq b$$

Applying the boundary condition $w(r = a) = 0$, yields:

$$h = \frac{1}{4S}\left(\Delta P\, a^2 - P_{att} b^2 \left(1 + log\left(\frac{a^2}{b^2}\right)\right)\right) \qquad (1)$$

Finally,

$$w = \frac{1}{4S}\left(\Delta P(a^2 - r^2) - P_{int}(b^2 - r^2) - P_{att} b^2 log\left(\frac{a^2}{b^2}\right)\right) \qquad r < b \qquad (2)$$

$$w = \frac{1}{4S}\left(\Delta P(a^2 - r^2) + P_{att} b^2 log\left(\frac{r^2}{a^2}\right)\right) \qquad r \geq b \qquad (3)$$

We assume that the membrane is in an equi-biaxial state, then $S_r = S_t$ and $\epsilon_r = \epsilon_t = \frac{S}{Et/(1-\nu)}$ and:

$$\epsilon_r + \epsilon_t = \frac{du}{dr} + \frac{u}{r} + \frac{1}{2}\left(\frac{dw}{dr}\right)^2 = \frac{2\, S_r}{Et/(1-\nu)}$$

Integrating with respect to an area element $2\pi r dr$ over (0, a), yields:

$$\int_0^a d(ur) + \int_0^a \frac{r}{2}\left(\frac{dw}{dr}\right)^2 dr = \frac{2\, S_r}{Et/(1-\nu)} \int_0^a r dr$$

The first integral on the LHS is zero due to the boundary conditions and thus:

$$S_r\, S^2 = \frac{Et}{32\, a^2(1-v)}\left((\Delta P - P_{att})^2 b^4 + \Delta P^2\left(a^4 - b^4\right) + P_{att}^2 b^4 log\left(\frac{a^4}{b^4}\right) - 4\,\Delta P\, P_{att} b^2\left(a^2 - b^2\right)\right) \qquad (4)$$

In order to obtain the condition for pull-in we eliminate S_r and S from eqs. (1) and (4) results in an equation for h in terms of a, b, Et, v, β, S_0, P_{att} and ΔP; in our experimental configuration all of these are known except ΔP and S_0. When we specify a particular value of S_0 this yields an expression for the load-deflection behaviour, i.e., ΔP vs. h.

$$\frac{Et}{32\, a^2(1-v)}\left((\Delta P - P_{att})^2 b^4 + \Delta P^2\left(a^4 - b^4\right) + P_{att}^2 b^4 log\left(\frac{a^4}{b^4}\right) - 4\,\Delta P\, P_{att} b^2\left(a^2 - b^2\right)\right) + \left(S_0\left(\frac{1}{4h}\left(\Delta P\, a^2 - P_{att} b^2\left(1 + log\left(\frac{a^2}{b^2}\right)\right)\right)\right)^2\right) = \left(\frac{1}{4h}\left(\Delta P\, a^2 - P_{att} b^2\left(1 + log\left(\frac{a^2}{b^2}\right)\right)\right)\right)^3 \qquad (5)$$

Consistent with the van der Waals (vdW) form, we assume P_{att} is given by a power law of the form,

$$P_{att} = \frac{\beta}{h^4}$$

The pull-in condition occurs at the limit point:

$$\frac{d\Delta P}{dh} = 0 \qquad (6)$$

which yields a unique ΔP and S_0 when β and h are specified.

Finite Element Simulations

To validate the analytical model, we also carried out high-fidelity finite element simulations of the experimental configuration using the code Abaqus where we remove the assumptions used to develop the analytical model. The model used in the simulations is shown in Figure S3 (b). Axisymmetric shell elements (that permit both bending and membrane behaviour) were used and the Young's modulus and Poisson's ratio were set to 1 TPa[3] and 0.16[4] respectively. The outer edge of the membrane is pinned and the substrate/post is modelled as a fixed analytical rigid body. Since it is known that pressurized graphene behaves like a membrane and bending plays a negligible role in its mechanics[8,9], the value of the bending modulus and slope near the boundary is found to be irrelevant in these simulations. A prescribed initial tension is applied and the attractive interactions between the substrate and the membrane are modelled as surface-to-surface contact/adhesive interactions with the substrate being the master surface. The contact interaction properties are supplied through the user subroutine "UINTER" of Abaqus[10]. The slave nodes experience a tensile (attractive) contact stress (σ_z) only in the vertical direction given by,

$$\sigma_z(r) = -\frac{\beta}{w(r)^4}$$

Here, β is a parameter and w is the deflection of the node measured from the substrate. Both σ_z and w are functions of the radial position, in contrast to the analytical model where they are assumed to be independent of position.

The simulation is split into two steps – both static steps with nonlinear geometric effects included. In the step 1, the contact/adhesive interactions are suppressed and the membrane is allowed to deform under the influence of a uniform pressure load acting on the entire area of the suspended membrane. The magnitude of this load is set such that the deflection is just high enough to neglect the interaction pressure if the interactions were not suppressed. This simulates the state of affairs at the beginning of the experiment before the gas begins to leak from the cavity. In the second step, which is a Static-Riks step[10], a second uniform pressure load is added with the same magnitude as the previous pressure load but in the opposite direction and the surface interactions between the substrate and the membrane are switched on. Hence at a given increment during the step, apart from the force due to the contact interactions, the membrane has the uniform pressure load from the previous step and a uniform pressure in the opposite direction whose value is given by the load proportionality factor. The superposition of these two uniform pressure loads mimics the leaking of the gas in the experiment. As the simulation progresses, the load across the membrane decreases and it comes closer to the substrate. This increases the interaction between the post and membrane. The results of this step are plotted in Figure 2a of the main text. It can be seen that the load across the membrane initially decreases until a limit point is reached and then it starts increasing. The limit point gives the pull-in distance and the pressure at which it occurs. The configurations below the limit point can't be achieved in a load controlled experiment, but suggest that system has two possible equilibrium configurations at a given pressure load greater than

the pull-in pressure. Careful comparison of the analytical and finite element simulation results (Fig. S4) shows that the analytical result is an accurate description of the physical phenomena as long as the substrate/post size is small compared to the size of the suspended membrane.

Calculation of β

Using the analytical model described above, we calculate the values of β assuming a range of initial tension, S_0. Previous results on mechanically exfoliated monolayer and few layer graphene found S_0 in the range of 0.03 - 0.15 N/m where the average values was S_0 =0.07 N/m[5–7]. Figure S5a shows calculated β for different S_0 (0.03, 0.05, 0.09 N/m). This range also marks the shaded boundaries for the theoretically calculated pull-in distance in Fig. 3.

Calculation of α, γ

The same analytical model used to calculate β can be applied to α and γ, where γ is a constant similar to α and β assuming $P_{att} = \gamma/h^3$. The inverse cubic dependence for the interfacial interactions can arise due to vdW interactions between thick graphene membranes and the substrate. Calculated α and γ with S_0 = 0.03, 0.05, 0.09 N/m is shown in Fig. S5b and Fig. S5c. The calculated α for all the devices measured is plotted in Fig. S6a assuming S_0 = 0.07 N/m. The same analysis is done with γ shown in Fig. S6b. We also plot pull-in distance (h) versus post diameter ($2b$) for this power law and compare it with $P_{att} = \beta/h^4$ and the experimental data in Fig. S7. Even though the plot fits

experimental data closely for 2-4 layers graphene membrane, it does not fit the data from monolayer graphene membranes as well.

Deformation of graphene membrane by vdw force

The extreme flexibility of the suspended graphene coupled with the large magnitude of the interfacial force at these short separations shows up as a statically deformed membrane right before pull-in for some devices. This is especially evident for a graphene membrane with a small inner post – more localized force- and a large outer diameter – more flexible graphene (Fig. S8). The AFM image shows a graphene membrane locally deformed at its center shortly before pull-in (Fig. S8a). The AFM line cut through the center (Fig. S8b) shows this deformation to be about 2 nm. This deformation is further verified by the analytical model which shows a number of stable configurations for graphene membranes deformed by P_{att} at these dimensions and separations (Fig. S8c).

Supplementary References:

1. Koh, Y. K., Bae, M.-H., Cahill, D. G. & Pop, E. Reliably counting atomic planes of few-layer graphene (n > 4). *ACS nano* **5**, 269–74 (2011).

2. Saif, M. T. A., Alaca, B. E. & Sehitoglu, H. Analytical modeling of electrostatic membrane actuator for micro pumps. *Microelectromechanical Systems, Journal of* **8**, 335–345 (1999).

3. Lee, C., Wei, X., Kysar, J. W. & Hone, J. Measurement of the Elastic Properties and Intrinsic Strength of Monolayer Graphene . *Science* **321** , 385–388 (2008).

4. Blakslee, O. L., Proctor, D. G., Seldin, E. J., Spence, G. B. & Weng, T. Elastic Constants of Compression-Annealed Pyrolytic Graphite. *Journal of Applied Physics* **41**, 3373–3382 (1970).

5. Bunch, J. S. *et al.* Impermeable atomic membranes from graphene sheets. *Nano letters* **8**, 2458–62 (2008).

6. Barton, R. A. *et al.* High, Size-Dependent Quality Factor in an Array of Graphene Mechanical Resonators. *Nano Letters* **11**, 1232–1236 (2011).

7. Wang, L. *et al.* Ultrathin Oxide Films by Atomic Layer Deposition on Graphene. *Nano Letters* (2012).doi:10.1021/nl3014956

8. Koenig, S. P., Boddeti, N. G., Dunn, M. L. & Bunch, J. S. Ultrastrong adhesion of graphene membranes. *Nat Nano* **6**, 543–546 (2011).

9. Zong, Z.; Chen, C.-L.; Dokmeci, M. R.; Wan, K.-t. *Journal of Applied Physics* 2010, 107, (2), 026104-3.

10. Hibbitt, K., Sorensen, ABAQUS/Standard: user's manual. Dassault Systèmes Simulia Corp.: Providence, RI, USA, 2011.

Supplementary Figure Captions

Figure S1: Determining the number of layers

(a) Optical image showing one of the graphene flakes corresponding to some of the samples measured in Fig. 1e. The colored circles denote the location at which Raman spectroscopy was taken (black-1 layer, red-2 layers, green-3 layers, blue-4 layers, and cyan-5 layers).

(b) Raman spectrum for the graphene flake in (a). The color of each curve corresponds to Raman spectrum taken at the corresponding colored circle in the optical image.

(c) Ratio of the integrated intensity of the first order silicon peak I(Si) and the graphene G peak, I(G) (i.e. I(G)/I(Si) for the Raman spectrum in (b).

Figure S2: Additional Raman spectrum

(a) Optical image showing a few layer graphene flake on Au coating. The blue circles denote the location at which Raman spectroscopy was taken.

(b) Raman spectrum for 2-5 layers graphene flakes on Au coating through 5 μm wells.

(c) Ratio of the integrated intensity of the first order silicon peak *I*(Si) and the graphene G peak, *I*(G) (i.e. *I*(G)/*I*(Si) for the Raman spectrum in (b).

Figure S3: Schematic of the model

(a) Schematics showing the equilibrium condition for the two regions of the membrane.

(b) Schematic of the model used for finite element analysis simulations.

Figure S4: Comparison of analytical solution and finite element simulations

(a) Plots comparing p vs h behavior as obtained from the FE simulations (solid curve) and the analytical calculations (dashed curve) with a = 1.5 μm, b = 0.25 μm, Et = 340 N/m, ν = 0.16, S_0 = 0.07 N/m and β = 0.02 nN-nm^2.

(b) The deflection profiles at different pressures (solid – FE, dashed – Analytical) (Red – 10.38 kPa, Blue – 6.12 kPa, Green – 1.72 kPa and Magenta – 2.61 kPa). For convenience, the corresponding points on p vs h plot are also shown. (c) and (d) The same as (a) and (b) except b = 0.75 μm. The different pressures used in this case are: Red – 10.39 kPa, Blue – 6.14 kPa, Green – 2.63 kPa and Magenta – 3.70 kPa.

Figure S5: α, β, γ vs. number of layers

(a) The calculated values of β vs. number of layers assuming a model where the force responsible for pull-in has the form $P_{att} = \beta/h^4$ with different initial tension S_0 = 0.03 N/m, S_0 = 0.05 N/m, S_0 = 0.09 N/m.

(b) The calculated values of α vs. number of layers assuming a model where the force responsible for pull-in has the form $P_{att} = \alpha/h^2$ with different initial tension S_0 = 0.03 N/m, S_0 = 0.05 N/m, S_0 = 0.09 N/m.

(c) The calculated values of γ vs. number of layers assuming a model where the force responsible for pull-in has the form $P_{att} = \gamma/h^3$ with different initial tension S_0 = 0.03 N/m, S_0 = 0.05 N/m, S_0 = 0.09 N/m.

Figure S6: α, γ for all devices measured.

(a) Calculated α for all the devices measured assuming S_0 = 0.07 N/m; (same color scheme as Fig. S5a).

(b) Calculated γ for all the devices measured assuming S_0 = 0.07 N/m; (same color scheme as Fig. S5a).

Figure S7: Scaling of the Pull in Distance with P_{att}

Pull in distance, h_0, vs. inner diameter, 2b, for a) 1 layer b) 2 layer c) 3 layer d) 4 layer graphene flakes (verified by Raman spectroscopy) with identical outer diameter but different inner diameters. The black and blue shaded lines are the calculated results for 2 different power law dependences $P_{att} = \beta/h^4$ (black) and $P_{att} = \alpha/h^3$ (blue) with S_0 = 0.03 – 0.09 N/m. The values of β and γ are listed in Fig. S5. a) (inset) Optical image of 2 of the measured monolayer devices. The scale bar = 5 μm.

Figure S8: Deforming a Graphene Membrane with the vdw Force

(a) An atomic force microscope image showing a close up view of the top part of the pressurized graphene membrane right before pull-in showing the deformation at the center of the membrane resulting from the vdw force.

(b) A line cut through the center of the image in (a).

(c) Calculated deflection vs. position through the center of a graphene membrane using the analytical model, for varying S_0.

Figure

Fig.S1

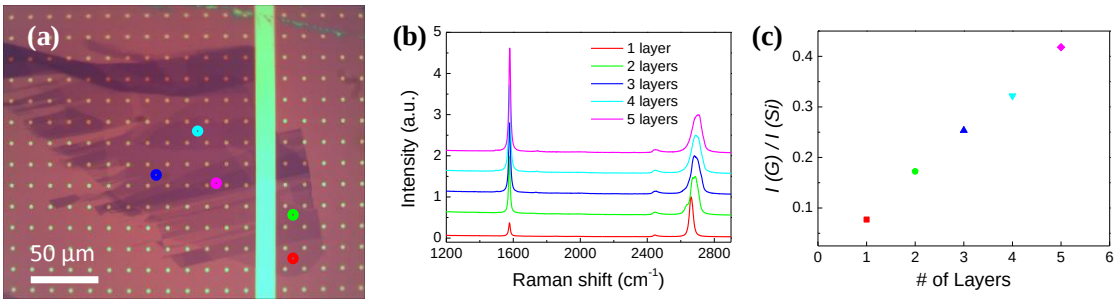

Fig.S2

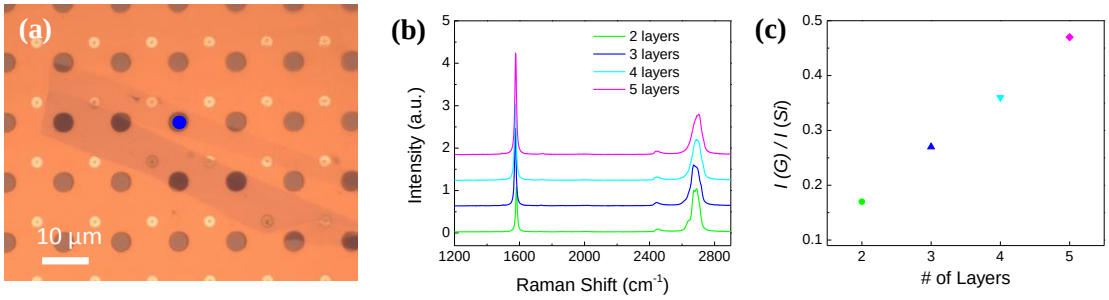
(a)
10 μm
(b)
2 layers
3 layers
4 layers
5 layers
Intensity (a.u.)
Raman Shift (cm-1)
(c)
I (G) / I (Si)
# of Layers

Fig.S3

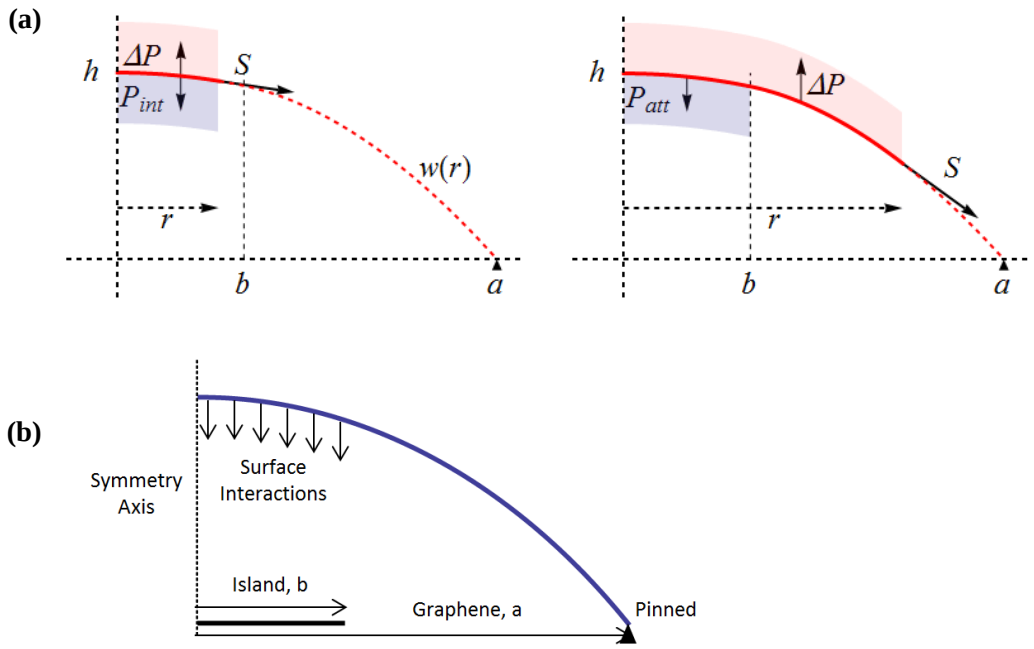
(a)
h
ΔP
P int
S
w(r)
r
b
a
h
P att
ΔP
S
r
b
a
(b)
Symmetry Axis
Surface Interactions
Island, b
Graphene, a
Pinned

Fig.S4

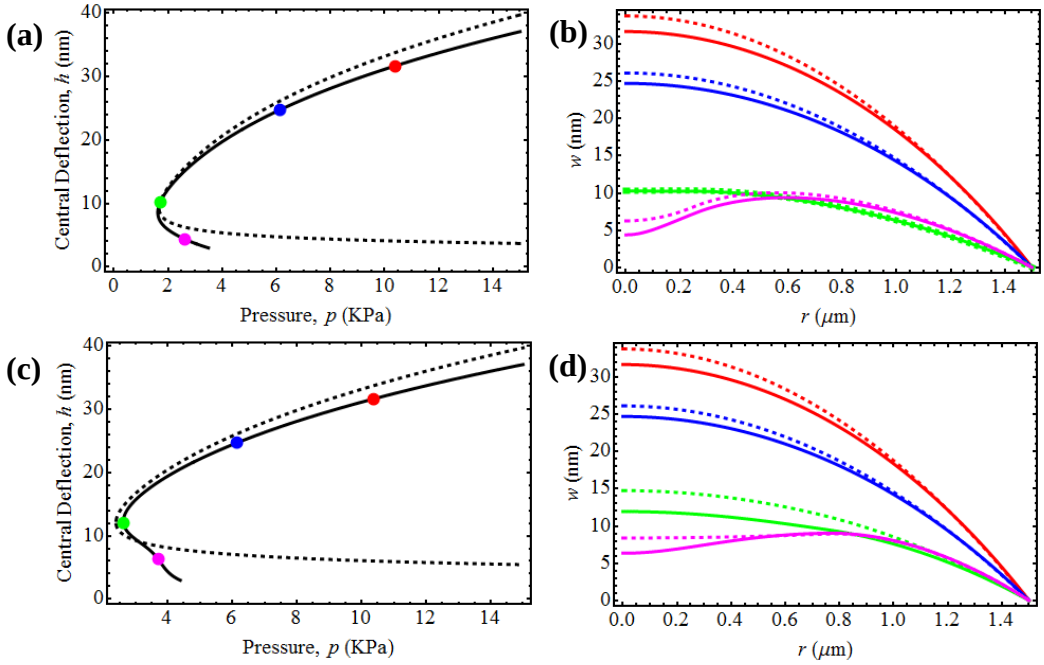
(a)
Central Deflection, h (nm)
Pressure, p (KPa)
(b)
w (nm)
r (μm)
(c)
Central Deflection, h (nm)
Pressure, p (KPa)
(d)
w (nm)
r (μm)

Fig.S5

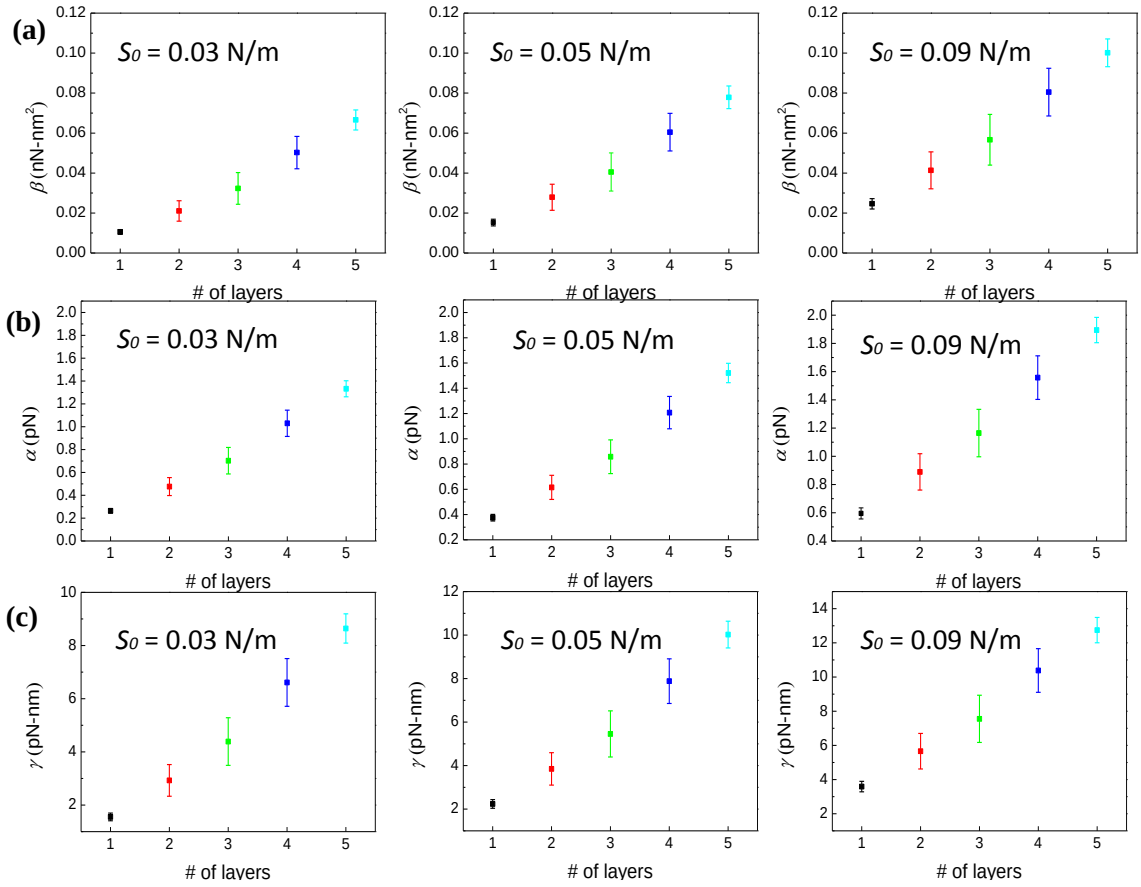
(a)
S_0 = 0.03 N/m
S_0 = 0.05 N/m
S_0 = 0.09 N/m
β (nN-nm^2)
(b)
α (pN)
(c)
γ (pN-nm)
# of layers

Fig.S6

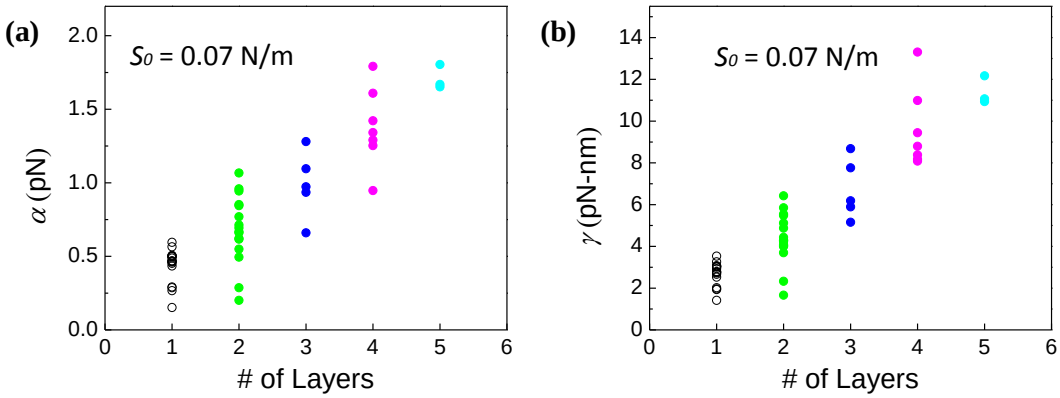

Fig.S7

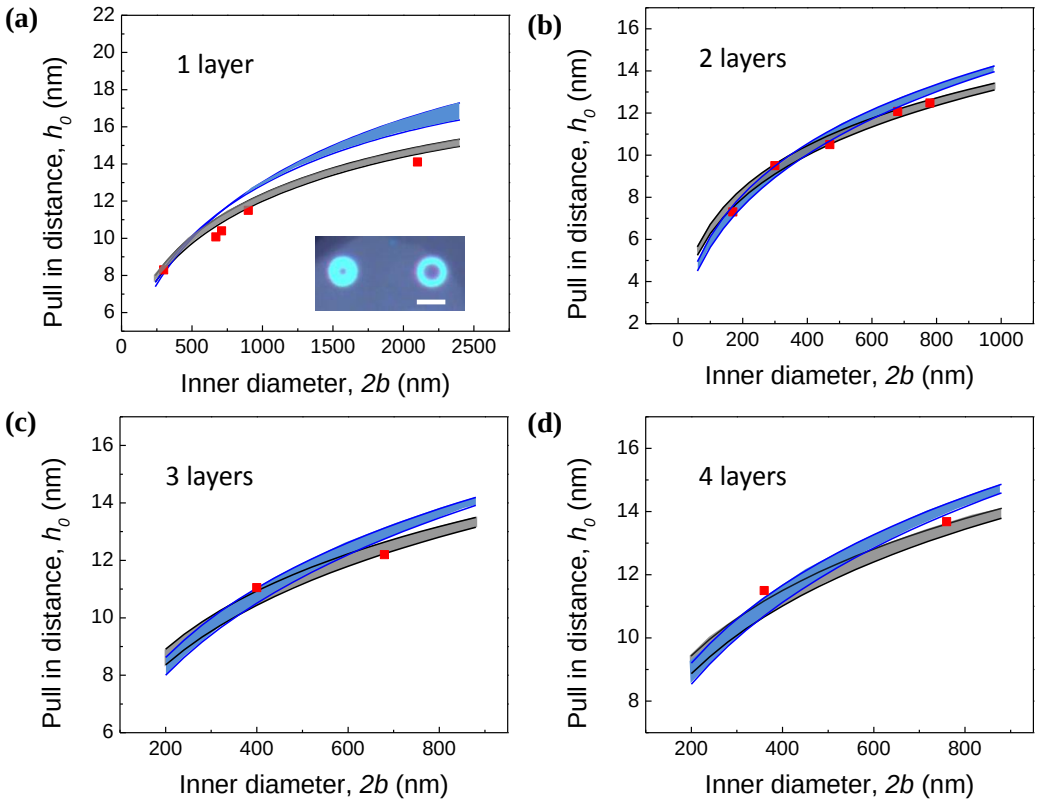
(a)
1 layer
Pull in distance, h_0 (nm)
Inner diameter, 2b (nm)
(b)
2 layers
Pull in distance, h_0 (nm)
Inner diameter, 2b (nm)
(c)
3 layers
Pull in distance, h_0 (nm)
Inner diameter, 2b (nm)
(d)
4 layers
Pull in distance, h_0 (nm)
Inner diameter, 2b (nm)

Fig. S8

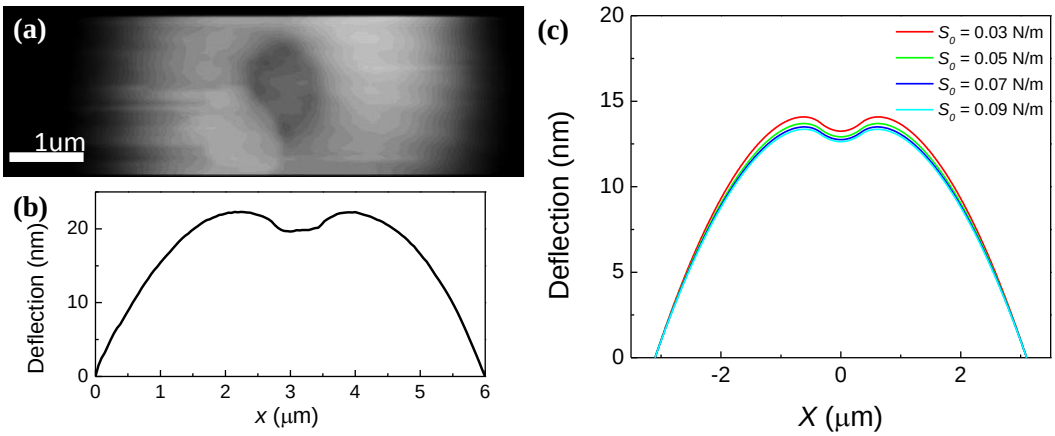
(a)
1um
(b)
Deflection (nm)
x (μm)
(c)
Deflection (nm)
X (μm)
S_0 = 0.03 N/m
S_0 = 0.05 N/m
S_0 = 0.07 N/m
S_0 = 0.09 N/m